Ground-state energy density, susceptibility, and Wilson ratio of a two-dimensional disordered quantum spin system

J.-H. Peng, D.-R. Tan, and F.-J. Jiang*

Department of Physics, National Taiwan Normal University, 88, Sec.4, Ting-Chou Road, Taipei 116, Taiwan

(Received 1 September 2020; revised 21 October 2020; accepted 27 November 2020; published 21 December 2020)

A two-dimensional (2D) spin-1/2 antiferromagnetic Heisenberg model with a specific kind of quenched disorder is investigated, using the first-principles nonperturbative quantum Monte Carlo calculations (QMCs). The employed disorder distribution has a tunable parameter p which can be considered as a measure of randomness ($p = 0$ correponds to the clean model). Through large-scale QMCs, the dynamic critical exponents z, the ground-state energy densities E_0, and the Wilson ratios W of various p are determined with high precision. Interestingly, we find that the p dependencies of z and W are likely to be complementary to each other. For instance, while the z values of $0.4 \leqslant p \leqslant 0.9$ match well among themselves and are statistically different from that of $p = 0$, the W values for $p < 0.7$ are in reasonably good agreement with $W \sim 0.1243$ of the clean case. Surprisingly, our study indicates that a threshold of randomness, p_W, associated with W exists. In particular, beyond this threshold the magnitude of W grows with p. This is somehow counterintuitive since one expects the spin correlations should diminish accordingly. Similarly, there is a threshold p_z related to z after which a constant value is obtained for z. The results presented here are not only interesting from a theoretical perspective but also can serve as benchmarks for future related studies.

DOI: 10.1103/PhysRevB.102.214206

I. INTRODUCTION

Spatial dimension two is extraordinary from a theoretical point of view. This is because according to the famous Mermin-Wagner theorem, for finite systems with short-range interactions, continuous symmetries cannot be broken spontaneously at any temperature $T > 0$ [1–6]. As a result, for two-dimensional (2D) quantum spin antiferromagnets (AF), the associated studies have been focusing on certain exotic finite-temperature properties of the systems. Particularly, several universal quantities have been predicted and verified numerically. Such a temperature region where these unusual universal features exist is called the quantum critical regime (QCR) in the literature and has been explored in detail during the past few decades [7–19].

For 2D quantum spin AF systems, whenever QCR is mentioned, it typically refers to a finite-temperature region. However, such an exotic regime extends to zero temperature at a quantum critical point (QCP). In addition, the (finite-T) region above a QCP is where these profound characteristics can be uncovered the most clearly [14,19].

A physical observable, namely, the spin-wave velocity c, plays an important role in those mentioned universal quantities of QCR for the 2D spin-1/2 antiferromagnets. For instance, the value of c without doubt has great impact on the determination of two universal quantities of QCR, namely, $\chi_u c^2/T \sim 0.27\,185$ and $c/(T\xi) \sim 1.04$. Here χ_u and ξ are the uniform susceptibility and the correlation length, respectively [10,14,19]. In the phase with long-range antiferromagnetic order, c can be calculated efficiently using the spatial and the temporal winding numbers squared [18,20,21].

Considering a clean 2D spin-1/2 AF which comes with a given spatial arrangement of two types of antiferromagnetic couplings, J' and J ($J' > J$), by tuning the ratio J'/J (i.e., the system is dimerized) a QCP may appear when J'/J exceeds a certain value, $(J'/J)_c$. The dynamic critical exponent z associated with such a kind of QCP takes the value of 1. For a QCP g_c, which is obtained by varying the associated parameter g, the physical quantity c scales as $c \propto (g_c - g)^{\nu(z-1)}$ close to g_c [10,13], where ν is the correlation length exponent. As a result, c is a constant when the related z of a QCP is 1. For 2D quantum AF systems, the QCPs induced by dimerization introduced above belong exactly to this case. When disorder is present, $z > 1$ and c is zero at g_c. Consequently, certain universal quantities of QCR cannot be calculated in a direct manner for disordered systems.

While for a 2D disordered quantum spin antiferromagnet certain quantities of QCR such as $\chi_u c^2/T$ cannot be directly accessed, some observables do not encounter the difficulty that c cannot be calculated with ease. One of them, namely, the Wilson ratio W [10,17,18], is one of the main topics of our study presented here.

W is a dimensionless quantity associated with the susceptibility and the specific heat. Particularly, it characterizes the relation between various types of interactions and plays an important role in heavy fermion systems and Kondo lattices [22–24]. By replacing the susceptibility with other quantities (like the compressibility), one can study the Wilson ratios of other systems such as the disordered (hard core) Bose-Hubbard model, which is a model that has been investigated in great detail in the literature [25–28]. Interestingly, despite

*fjjiang@ntnu.edu.tw

its importance, the relevant (numerical) studies of W for spin systems are rather limited, and how this quantity responds to the presence of disorder in the systems has not been explored (in detail) yet.

When quenched disorder is introduced into a clean spin system, several physical quantities such as those mentioned above may be affected. Moreover, understanding the dependence of certain observables on the strength of randomness is an interesting research topic to investigate as well. For instance, the study of Ref. [29] leads to an exotic scenario of ν with respect to the strength of a specific disorder distribution. Here we carry such an exploration further by focusing on W. We would like to point out that, since disorders often present in real materials, our investigation is important as well from a practicing point of view.

Due to these described intriguing motivations, in this study we investigate the behavior of W with respect to the strength of randomness, which is controlled by the parameter $p \geqslant 0$, of an employed disorder distribution. Here $p = 0$ corresponds to the clean case. Apart from W, the dynamic critical exponents z and the ground-state energy densities E_0 of several values of p considered in this study are determined as well.

To carry out the proposed investigation, we have performed a large-scale quantum Monte Carlo calculation (QMC). In addition, several p are considered. For each of the studied p there is an associated critical point, $g_c(p)$, beyond which the long-range antiferromagnetic order is destroyed. In this investigation, the simulations are done at the these critical points $g_c(p)$.

Based on our numerical results, we find the magnitude of E_0 grows monotonically with $g_c(p)$ (hence, p as well since $g_c(p) \propto p$ as shown in Ref. [29]), similar to that of the correlation length exponent ν [29]. Interestingly, the p dependencies of z and W are likely to be complementary to each other. For instance, while the z values of $0.4 \leqslant p \leqslant 0.9$ match well among themselves and are statistically different from $z = 1$, which corresponds to the clean system, the W values for $p < 0.7$ are in reasonably good agreement with that of $p = 0$ ($W \sim 0.1243$).

The scenario of W indicates that there is a threshold of randomness such that a randomness with less strength has the same influence on both the susceptibility and the specific heat. Moreover, the enhancement of W for $p \geqslant 0.7$ implies that, beyond the mentioned threshold, the correlations between spins are getting stronger and stronger with p. This is confirmed by the p dependence of χ_u obtained here and is rather counterintuitive since spin correlations should diminish with the strength of randomness.

Finally, the subtlety of calculating these physical quantities for a disordered system is demonstrated here as well. Our investigation is important and interesting in itself from a theoretical perspective. In particular, the obtained outcomes can be used as benchmarks for future related studies.

The rest of this paper is organized as follows. In Sect. II the studied model, the employed disorder distribution, and the relevant observables are described. We then present our numerical results, including the evidence for the mentioned complementary relation for z and W, in Sec. III. Finally, in Sec. IV we present discussions and conclusions.

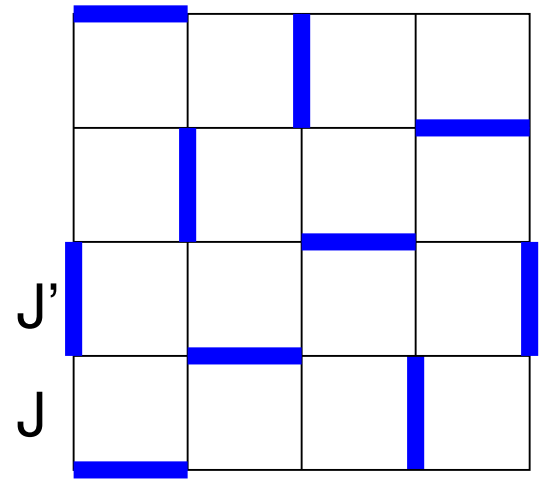

FIG. 1. The 2D dimerized spin-1/2 herringbone Heisenberg model on the square lattice investigated in this study [29]. The antiferromagnetic coupling strengths for the thick and thin bonds are J' and J, respectively.

II. MICROSCOPIC MODELS AND OBSERVABLES

The model investigated in our study has been described in detail in Refs. [29,30]. Here we briefly summarize certain technical perspectives of the considered system. The Hamiltonian of the investigated 2D disordered spin-1/2 herringbone Heisenberg model (on a square lattice) is given by

$$H = \sum_{\langle ij \rangle} J\, \vec{S}_i \cdot \vec{S}_j + \sum_{\langle i'j' \rangle} J'\, \vec{S}_{i'} \cdot \vec{S}_{j'}, \tag{1}$$

where J (which is set to 1 here) and J' are the antiferromagnetic couplings (bonds) connecting nearest-neighbor spins $\langle ij \rangle$ and $\langle i'j' \rangle$, respectively, and $\vec{S}_i$ is the spin-1/2 operator at site i. In this study we use the convention $J' > J$. Figure 1 is a cartoon representation of the considered model. The quenched disorder introduced into the system is based on the one employed in Refs. [29,30]. Specifically, for every bold bond in Fig. 1, its antiferromagnetic strength J' takes the value of $1 + (g-1)(1+p)$ or $1 + (g-1)(1-p)$ with equal probability. Here $g > 1$ and $0 \leqslant p \leqslant 1$. With the used conventions, the average and the difference for these two types of bold bonds J' are given by g and $2p(g-1)$, respectively. In addition, p can be thought of as a measure for the disorder of the studied model.

To perform the proposed calculations to determine the ground-state energy density E_0, the dynamic critical exponent z, and the Wilson ratio W for the considered disordered system (with various p), the uniform susceptibility χ_u, the internal energy density E, and the specific heat C_V (as functions of the temperature T or the inverse temperature β) are measured in our simulations.

The uniform susceptibility χ_u is defined by

$$\chi_u = \frac{\beta}{L^2} \left\langle \left(\sum_i S_i^z \right)^2 \right\rangle, \tag{2}$$

where β and L are the inverse temperature and the linear box size used in the simulations, respectively. Furthermore, the internal energy density E and the specific heat C_V are given

as

$$E = \frac{1}{L^2}\langle H\rangle, \tag{3}$$

$$C_V = \frac{\partial E}{\partial T}. \tag{4}$$

Using these observables, E_0, z, and W for various p of the studied disordered model can be determined with high precision.

III. THE NUMERICAL RESULTS

For each of the considered values of $p = 0.0$, 0.2, 0.4, 0.5, 0.6, 0.7, 0.8, and 0.9, to calculate the desired physical quantities, we have carried out a large-scale QMC using the stochastic series expansion (SSE) algorithm with a very efficient operator-loop update [31,32].

SSE is one of the elegant algorithms for simulating (quantum) spin systems and is based on an important sampling of the high-temperature series expansion of the partition function Z. It is well-documented in the literature and the associated codes in various programming languages are available publicly [33,34]. In the framework of SSE one considers the contribution from the terms of the expansion of Z in an intelligent way. Particularly, when the z direction is chosen to be the quantized direction, the associated Hamiltonian H is divided into diagonal (H_1 which contains S^z) and off-diagonal (H_2 which involves S^+S^- and S^-S^+) terms. Moreover, three updates, namely, the diagonal update (add and remove H_1), the operator-loop update (exchange H_1 and H_2), and the isolated spin flipping, are employed to efficiently sample the spin configuration space. For the readers who are interested in the technical details of implementing SSE in any programming language, we refer them to Ref. [32], which also contains many physical results obtained using SSE.

With SSE, the simulations are executed at the corresponding critical points $g_c(p)$ for the chosen p. In addition, depending on p and L (here $L = 128$ and 256 are considered), (around) 330 to (around) 1300 randomness configurations are generated. Each configuration (of bonds) is produced with its own random seed and then is used for all calculations involving the considered values of β. In particular, when the simulation (which consists of both the thermalization and the measurement processes) at an inverse temperature β_1 is done, the final state corresponding to β_1 is employed as the initial state for the thermalization associated with $\beta_2 = \beta_1 + \epsilon$. Here ϵ is some positive number and either 0.5 or 1.0 is adopted. This procedure is conducted for all the used values of β. With such a strategy, the equilibrium for any calculation of a considered β is reached with moderate effort.

A. The strategy of calculating the Wilson ratio W

In the framework of SSE, the quantities of internal energy density E and specific heat C_V can be obtained by [32]

$$E = -\frac{1}{L^2}\left(\langle n\rangle/\beta - \frac{1}{4}\sum_b J_b\right), \tag{5}$$

$$C_V = \frac{1}{L^2}(\langle n^2\rangle - \langle n\rangle^2 - \langle n\rangle), \tag{6}$$

respectively, where the summation is over all the bonds b, and n is the number of nonidentity operators in the SSE operators sequence (operators string).

Based on the large-N expansion of the relevant effective field theory, at the associated critical point it is predicted that for the clean systems the (leading) low-T behaviors of χ_u, E, and C_V are given by [10,18]

$$\chi_u \sim \frac{1.0760}{\pi c^2}T, \tag{7}$$

$$E \sim E_0 + \frac{2.8849}{\pi c^2}T^3, \tag{8}$$

$$C_V \sim \frac{8.6548}{\pi c^2}T^2, \tag{9}$$

respectively, where c is the spin-wave velocity. With these leading T dependencies of χ_u, E, and C_V, the Wilson ratio W can be expressed as

$$W = \frac{\chi_u T}{C_V} \sim 0.1243. \tag{10}$$

While C_V can be calculated directly from its definition $C_V = \partial E/\partial T$ [or $C_V = \frac{1}{L^2}(\langle n^2\rangle - \langle n\rangle^2 - \langle n\rangle)$], as shown in the literature, such a direct approach will lead to very noisy results at the region of low temperature [18]. In addition, the fact that c is zero at the QCP of a disordered system prevents one from determining c in a straightforward manner. Motivated by the method outlined in Ref. [18], here we calculate W through the following procedures.

First, from the β dependence of the internal energy density E, namely,

$$E(\beta) = E_0 + a\beta^{-1-2/z} \tag{11}$$

(here z is the dynamic critical exponent), one obtains a and z. Then the specific heat C_V, as a function of β, can be written as

$$C_V = a(1 + 2/z)\beta^{-2/z}. \tag{12}$$

Second, the β-dependence of χ_u is fitted to the expression

$$\chi_u(\beta) = b\beta^{1-2/z}. \tag{13}$$

Finally, using Eqs. (12) and (13), one arrives at the following formula for W:

$$W = \frac{b}{a(1 + 2/z)}. \tag{14}$$

In other words, instead of using C_V directly, here W is calculated through the coefficients z, a, and b obtained from fitting the data of E and χ_u to their expected β-dependence ansatzes, Eqs. (11) and (13).

B. The obtained χ_u and E from simulations

The obtained data of χ_u and $-E$ for $p = 0.0$, 0.4, 0.6, and 0.9 are depicted in Figs. 2, 3, 4, and 5. Both data of $L = 128$ and $L = 256$ are put in these figures in order to demonstrate that the outcomes of $L = 256$ are (most likely) sufficient for size convergence. The insets shown in these figures are

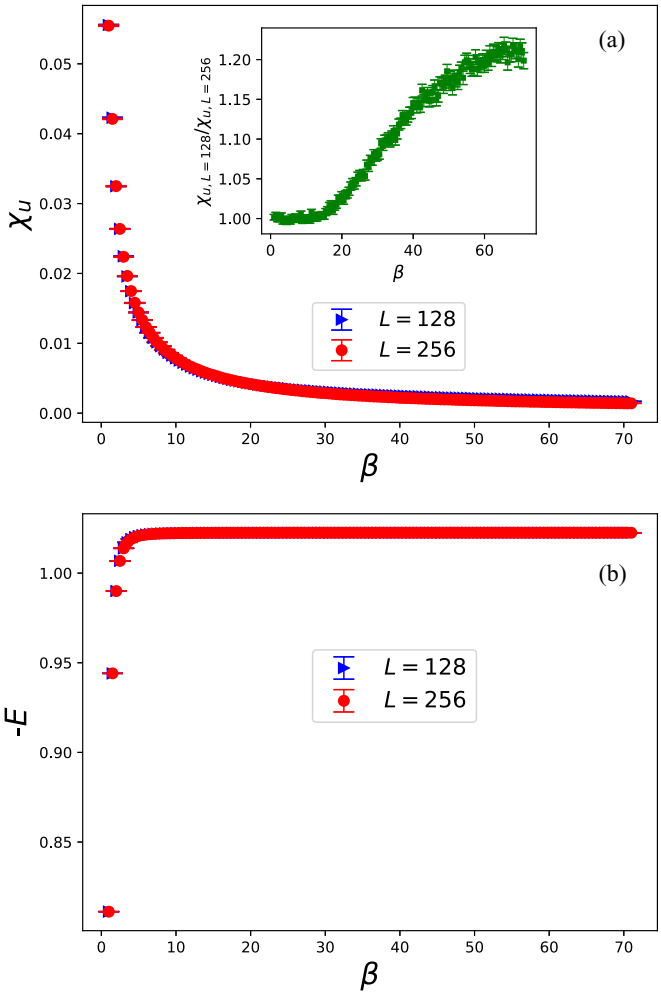

FIG. 2. χ_u (a) and negative (internal) energy density $-E$ (b) as functions of β for $p = 0.0$. The shown errors are the corresponding mean errors.

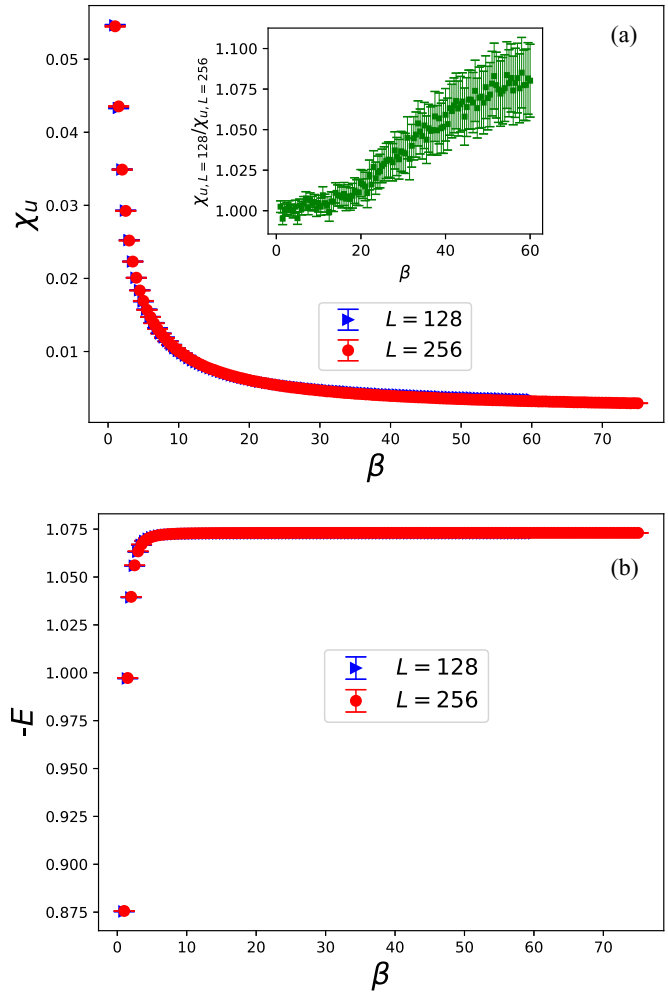

FIG. 3. χ_u (a) and negative (internal) energy density $-E$ (b) as functions of β for $p = 0.4$. The shown errors are the corresponding mean errors.

the ratios between the $L = 128$ and the $L = 256$ results of χ_u.

Interestingly, with a detailed investigation, we find that the main systematic impact on the determination of W is from χ_u. Moreover, the influence due to finite lattice for χ_u is less and less severe with p (see the insets of Figs. 2, 3, 4, and 5). Although the observables used to calculate the desired physical quantities do receive finite-size effects, we argue later that z, E_0, and W determined on $L = 256$ lattices, at least for the majority of the considered values of p, are free of such effects.

The approach to the calculations of W used here involves both χ_u and E. In particular, the coefficients a, z, and b appearing in Eqs. (11) and (13) determine the Wilson ratio W. In other words, both the fitting results of χ_u and E are required for our estimation of W. For all the used p in this study, we have simulated both $L = 128$ and $L = 256$ lattices. Hence, we carry out the needed fits using only either the $L = 128$ or the $L = 256$ data (of χ_u and E). With such a strategy one can understand the systematic impact due to the finite-size lattices used in the simulations.

C. The results associated with the clean model

For the clean model $p = 0$, it is well known that $z = 1$. Hence, z is fixed to 1 in our analysis for $p = 0$. As a result, the following ansatz,

$$\chi_u = a_0 + aT + a_1 T^2, \tag{15}$$

is considered to fit the χ_u data of $p = 0$. Apart from that, the formula used to fit the data of E for $p = 0$ is Eq. (11) with $z = 1$ as well.

By investigating the relevant data of $L = 128$ and $L = 256$, the finite-size effect begins to appear when $\beta > 16.0$. Therefore, the data of $L = 256$ with $\beta \leqslant 24.0$ are used for the fits. We have additionally carried out fits using the $L = 256$ data of $\beta \leqslant 20.0$ and have found that these new results lead to a value of W which agrees quantitatively with that obtained using the $L = 256$ data of $\beta \leqslant 24.0$. For data with a fixed range of β, in addition to taking care of the finite-size effect, the following procedures are adopted to calculate the corresponding W.

First, a bootstrap resampling (with respect to β) is conducted simultaneously for both χ_u and E. Second, fits for these obtained resampled data are performed. Finally, W is determined using the outcomes of these fits. In these mentioned

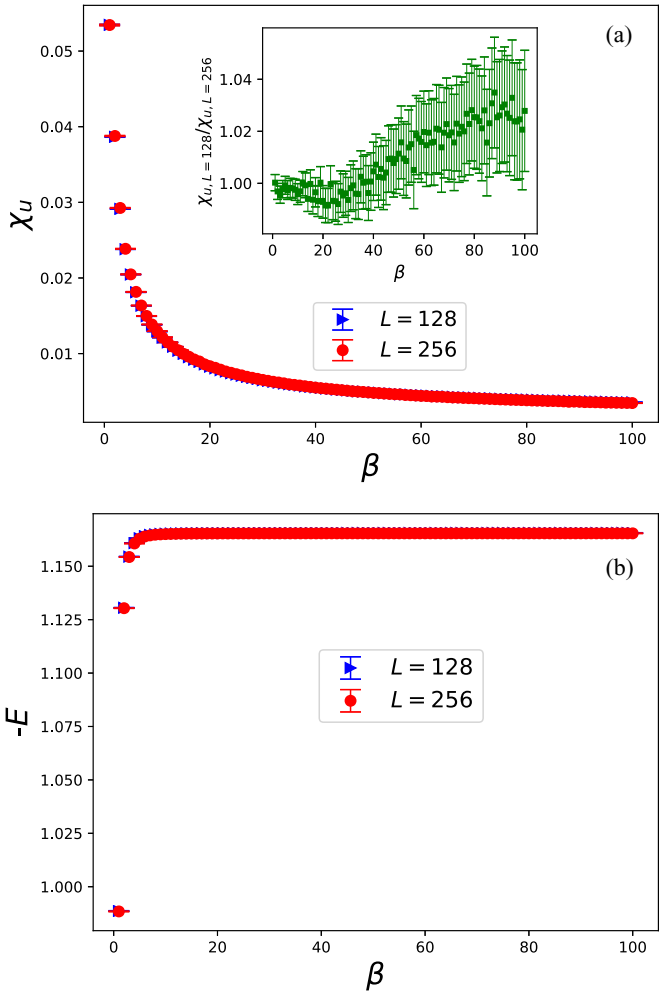

FIG. 4. χ_u (a) and negative (internal) energy density $-E$ (b) as functions of β for $p = 0.6$. The shown errors are the corresponding mean errors.

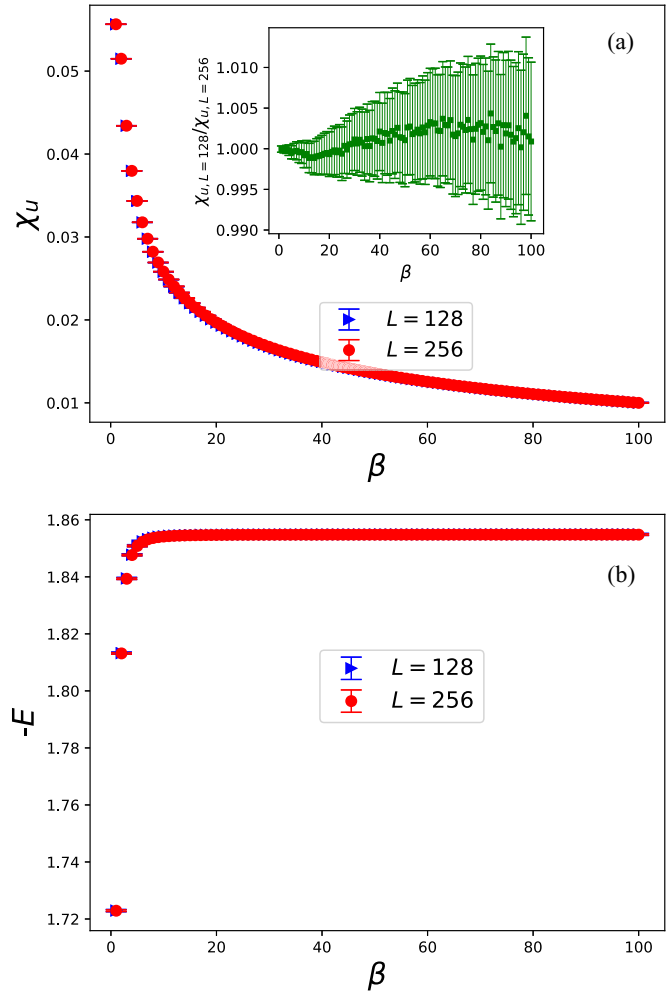

FIG. 5. χ_u (a) and negative (internal) energy density $-E$ (b) as functions of β for $p = 0.9$. The shown errors are the corresponding mean errors.

fits, Gaussian noises are considered as well. The above-described steps are carried out 20 000 times and only those outcomes with both χ^2/DOF (DOF stands for degrees of freedom) of the two fits (for χ_u and E) being smaller than 3.0 are included as the candidate results of W. The resulting W and its associated uncertainty quoted for this set of data with that given fixed range of β are the mean and the standard deviation of these candidate results.

We have conducted several calculations using various ranges of β (the minimum β used for these analyses satisfies $\beta \geqslant 4.0$), and each of these calculations comes with its own results (mean and uncertainty) for W. Moreover, to estimate the means and errors of the desired quantities appropriately, the weighted bootstrap resampling method is applied to all the mentioned results of W. Specifically, for every randomly generated data set (W_j, σ_{W_j}) obtained using the bootstrap procedure (σ_{W_j} is the standard deviation associated with W_j), the resulting mean is given by

$$\frac{\sum_i \frac{1}{\sigma_{W_i}^2} W_i}{\sum_i \frac{1}{\sigma_{W_i}^2}}. \tag{16}$$

The reason for the use of the above equation (called the weighted mean in this study) is as follows. Notice that data with large standard deviations are less accurately determined than those with small standard deviations. As a result, those large standard deviation data should contribute less weight to the determination of the associated mean.

After carrying out 20 000 weighted bootstrap resampling steps, the resulting W is estimated to be $W = 0.1238(3)$. The obtained $W = 0.1238(3)$ agrees very well with the theoretical prediction $W = 0.1243$. This confirms the validity of the procedures introduced above for the calculation of W.

The ground-state energy density for the clean model is calculated by the same procedure and is given as $E_0 = -1.022\,523(1)$.

D. The results of the disordered model with various randomness strengths p

Since each generated configuration is used for all simulations of the considered β, for a given set of $p > 0$ and L, the data themselves are correlated. Hence, to accurately estimate the associated errors for the coefficients in the fitting ansatzes,

one should employ the correlated least χ^2 method for the analysis. However, the stability of the correlated least χ^2 method varies and depends on the quality of the data used for the fits. Moreover, biased outcomes may be reached if the associated covariance matrix for a given data set contains eigenvalues which have very small magnitude. Using the rule of thumb that the considered ansatz to fit correlated data should contain as few (to be determined) parameters as possible, we adopt the following approach to calculate E_0, z, and W for $p > 0$.

First, the bootstrap resampling method is performed for the raw data resulting from the generated disordered configurations. Second, these resampled data are used to calculate the disordered average of χ_u and E, which are then considered for the relevant fits. Here the data employed for the fits of χ_u and E have different minimum values of β. Indeed, as can be seen from Figs. 3, 4, and 5, for all the considered $p > 0$ the associated E reaches its ground-state value E_0 quickly, while this is not the case for χ_u. As a result, it is more appropriate to use different minimum values of β for the fits of χ_u and E.

After carrying out the fit of χ_u, the obtained result of z is employed as an input for the fit of E. When both fits of χ_u and E are done, the resulting results are then put back to calculate the associated correlated χ^2/DOF. Here a cutoff for the eigenvalues of the associated covariance matrix is imposed in order to avoid biased results. These introduced steps are performed many times, and only those results which have correlated χ^2/DOF smaller than 3.0 for both the fits of χ_u and E are considered for later calculations. Finally, for each of the considered p, the above procedures have been applied to many data sets consisting of various ranges of β, i.e., the minimum of the used β varies, but the result corresponding to the largest β is always included in the analysis. For instance, for the fits of χ_u (E) associated with $p = 0.9$, while the largest β used is always $\beta_{\max} = 100$, the minimum β considered in the analyses consists of $\beta_{\min} = 20, 30, 40, 50, 60$ (12, 14, 16, 18, 20). Each of these sets (The whole set is denoted by S) has its own results (mean and standard deviation) of E_0, z, and W as well as the number of successful calculations.

For a considered p, the final quoted results of E_0, z, and W in this study are estimated by a bootstrap resampling procedure using the following formula to calculate the mean of every resampled data from S:

$$\frac{\sum_i N_i O_i/\sigma_{O_i}^2}{\sum_i N_i/\sigma_{O_i}^2}, \tag{17}$$

where $\{O_i\}$, $\{\sigma_{O_i}\}$, and $\{N_i\}$ stand for the randomly picked outcomes in S, the associated standard deviations, and the related numbers of (successful calculated) results of these chosen outcomes, respectively. Finally, such a resampling step is conducted several thousand times, and the numerical values presented here for these considered physical quantities are the resulting means and standard deviations (estimated conservatively) of this procedure. In conclusion, the analysis procedures for $p > 0$ can be summarized as follows.

(i) Calculate the disorder average of χ_u and E after carrying out a resampling of the original generated configurations.

(ii) Fit χ_u to the expression $b\beta^{1-2/z}$ using the conventional χ^2 method.

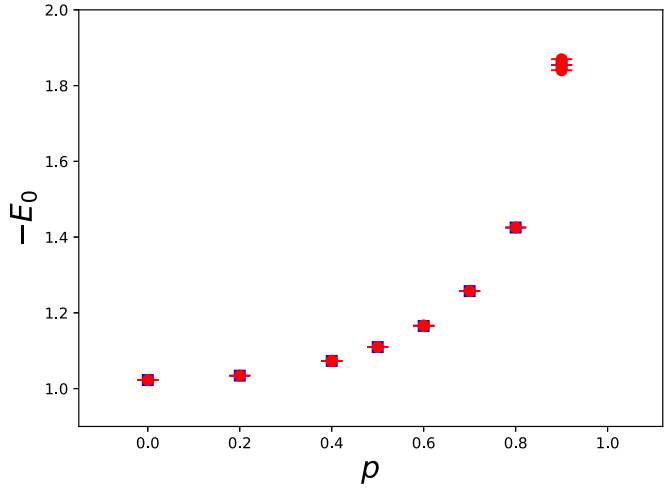

FIG. 6. $-E_0$ as functions of p. The results are obtained from the analysis using the correlated χ^2 described in the main text. The solid squares and solid circles are for $L = 256$ and $L = 128$, respectively. For some values of p, the $L = 128$ results contain those corresponding to g_c, the lower and upper bounds of g_c.

(iii) The obtained z is employed as an input for the (conventional χ^2) fit of E (the fitting ansatz for E is $E_0 + a\beta^{-1-2/z}$).

(iv) After the fits of χ_u and E are done, the obtained results are used to calculate the associated correlated χ^2/DOF.

(v) The repetition of above steps are applied to many data sets consisting of various ranges of β.

(vi) Obtain the means and the standard deviations from the results of every data set where both the correlated χ^2/DOF of χ_u and E are smaller than 3.0, and denote this collection as S.

(vii) Perform a resampling for the elements in S using Eq. (17).

The uncertainties of E_0 calculated by the described steps are much smaller than those of the original E_0 contained in S. Hence, for the data in S we have also calculated their associated weighted errors. The dominant one of these two estimations, namely, the standard deviations and the weighted errors, are the final values quoted here.

The $-E_0$, z, and W as functions of p calculated by the procedures introduced above are shown in Figs. 6, 7, and 8, respectively. The related results for the clean model are shown in these figures as well for comparison. The $-E_0$ as a function of p shows a monotonic behavior in magnitude, which is similar to that of the correlation length exponents ν obtained in Ref. [29]. Regarding the z values presented in Figure 7, one observes that the magnitude of z increases with p until p reaches a specific $p_c < 0.4$. For $p \geqslant 0.4$, all the calculated values of z lie between (around) 1.3 and (around) 1.4. If one takes into account the systematic errors due to the uncertainties of $g_c(p)$, then the z values for $p \geqslant 0.4$ are fairly close to each other. The solid and dashed lines in Fig. 7 represent the mean and standard deviation for all the values of z associated with $p \geqslant 0.4$ (including both those of $L = 128$ and $L = 256$). These guided lines justify the claim made above. This phenomenon is consistent with the one shown in Ref. [35], where the calculated z values corresponding to various parameters take a universal value. We would like to

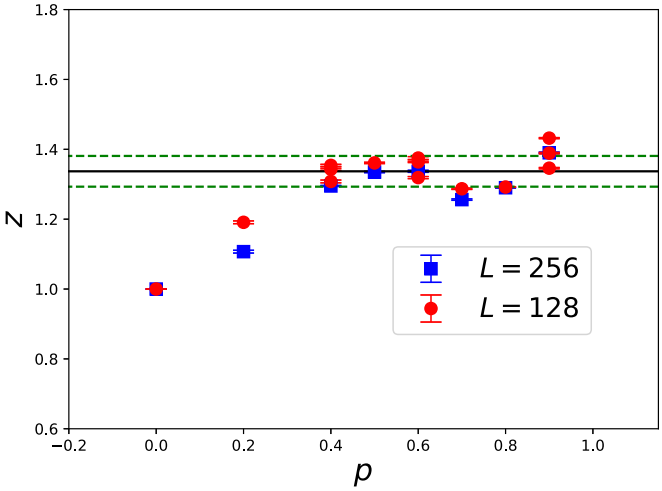

FIG. 7. z as functions of p. The results are obtained from the analysis using the correlated χ^2 described in the main text. The solid squares and solid circles are for $L = 256$ and $L = 128$, respectively. For some values of p, the $L = 128$ results contains those corresponding to g_c, the lower and upper bounds of g_c. The solid and dashed lines in the figure represent the mean and standard deviation for all the z values such that their associated p satisfy $p \geqslant 0.4$ (including both those of $L = 128$ and $L = 256$).

point out that when conducting the determination of z from χ_u, the obtained results are somehow a little bit sensitive to the considered fitting range of χ_u. This is the motivation for the use of the resampling procedures described above. In conclusion, our analysis indicates that it is subtle to calculate the quantity z and a careful strategy is needed.

In Fig. 8 we demonstrate both the $L = 128$ and $L = 256$ results of W as functions of p obtained from the analysis

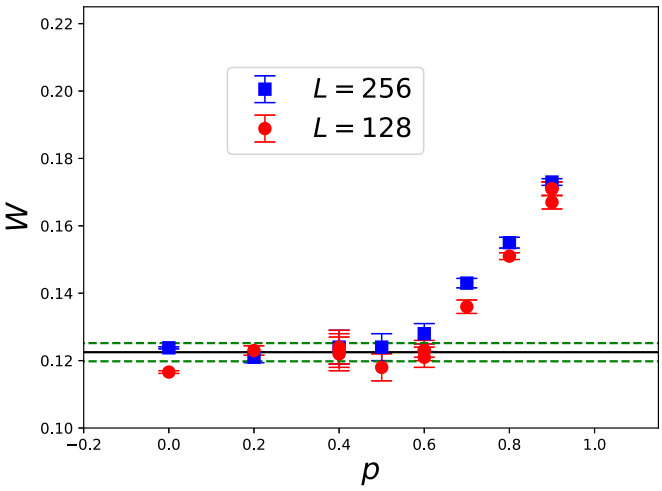

FIG. 8. W as functions of p. The results are obtained from the analysis using the correlated χ^2 described in the main text. The solid squares and solid circles are for $L = 256$ and $L = 128$, respectively. For some values of p, the $L = 128$ results contain those corresponding to g_c, the lower and upper bounds of g_c. The solid and dashed lines in the figure represent the mean and standard deviation for all the W values such that their corresponding p satisfy $p < 0.7$ (including both those of $L = 128$ and $L = 256$).

outlined previously. Intriguingly, similar to the scenario of z, for those W corresponding to $p < 0.7$, their values are more or less close to each other. The solid and dashed lines in the figure again stand for the mean and standard deviation for all the W with their associated p satisfying $p < 0.7$ (including both those of $L = 128$ and $L = 256$). Considering the impact resulting from the errors of $g_c(p)$, the scenario that W takes the same value (or at least values close to each other) for all the values of p such that $p < 0.7$ is probable. Interestingly, the correlation length exponent ν is beginning to fulfill the Harris criterion when $p > 0.8$ and this is where the magnitude of W increases sharply. This observation implies that there may exist a relation between W and the fulfillment of the Harris criterion.

Based on the outcomes presented in Figs. 6, 7, and 8, it is clear that for all the considered values of p the associated E_0 values receive negligible finite-size effect. Moreover, although small deviations are observed, the agreement between the $L = 128$ and the $L = 256$ results of z is very good for $p \geqslant 0.4$. This implies that the finite-size effects for those z values of $p \geqslant 0.4$ are most likely absent. A similar scenario applies to W as well. In other words, it is beyond reasonable doubt that the numerical values of W obtained on $L = 256$ lattices for all the considered p are the bulk ones.

Finally, the scenario of W implies the existence of a threshold of randomness, p_W. In particular, the randomness with strength smaller than this threshold effectively has no impact on χ_u and C_V. Apart from that, the enhancement of W for $p \geqslant 0.7$ indicates that, beyond the mentioned threshold, the correlations between spins are getting stronger and stronger with p. This phenomenon is surprising since spin correlations should diminish with the strength of randomness. Indeed, as can be seen from Figs. 4 and 5, the values of χ_u of $p = 0.9$ are larger than those associated with $p = 0.6$, implying stronger spin correlations for $p = 0.9$, which is a counterintuitive outcome.

IV. DISCUSSIONS AND CONCLUSIONS

In this study, we calculate the Wilson ratio W of a 2D spin-1/2 antiferromagnetic Heisenberg model with a specific quenched disorder, using the first-principles nonperturbative quantum Monte Carlo simulations. The employed disorder distribution has a tunable parameter p which can be considered as a measure of randomness. The W of the clean case and that of $p = 0.2$, 0.4, 0.5, 0.6, 0.7, 0.8, and 0.9 are determined with high precision. The critical dynamic exponents z and the ground-state energy densities E_0 are obtained as well.

Remarkably, for the considered system with the employed quenched disorder, the p dependencies of W and z seem to be complementary to each other. The obtained z values are likely to take a universal value for $p \geqslant 0.4$. Although this finding agrees with the outcomes determined in Ref. [35], we find it is probable that a threshold p_z exists and only beyond p_z will the described scenario of z (as a function of p) emerge. Besides z, the calculated W values for $0 < p < 0.7$ also have a trend of staying close to the result $W \sim 0.1243$ of the clean model ($p = 0$). Moreover, the value of W begins to increase sharply when p is approaching $p = 0.9$, where the Harris criterion is fulfilled. Considering the fact that under what conditions the Harris criterion is valid is still not known [35–46], the results

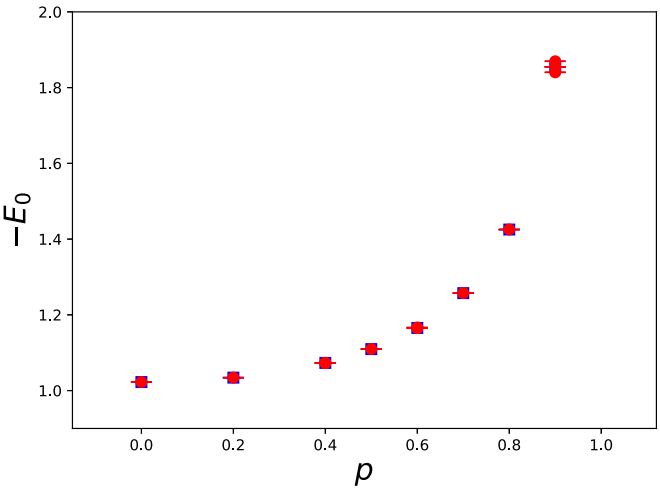

FIG. 9. $-E_0$ as functions of p. The results are obtained from the analysis using the conventional uncorrelated χ^2. The solid squares and solid circles are for $L = 256$ and $L = 128$, respectively. For some values of p, the $L = 128$ results contain those corresponding to g_c, the lower and upper bounds of g_c.

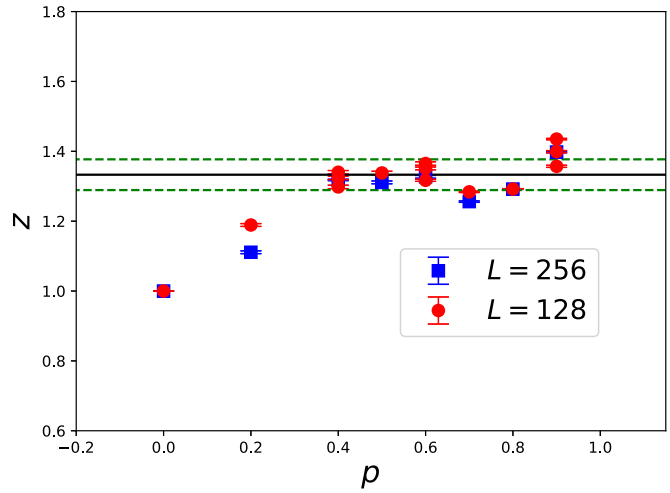

FIG. 10. z as functions of p. The results are obtained from the analysis using the conventional uncorrelated χ^2. The solid squares and solid circles are for $L = 256$ and $L = 128$, respectively. For some values of p, the $L = 128$ results contain those corresponding to g_c, the lower and upper bounds of g_c. The solid and dashed lines in the figure represent the mean and standard deviation for all the values of z such that their associated p values satisfy $p \geqslant 0.4$ (including both those of $L = 128$ and $L = 256$).

presented here may shed some light on setting up some useful guidelines to decide whether the Harris criterion is valid for a given disorder distribution.

In addition to the subtlety of calculating z described previously, the determination of W is extremely nontrivial as well. Indeed, the estimation of W here is based on Eq. (14), which contains two constants, a and b. Since a is a subleading coefficient in the associated ansatz, it is sensitive to the range of β used for the fits. Careful strategy and resampling procedures are conducted in this study in order to calculate W accurately.

If the correlations among the data of various values of β are ignored, then the same resampling steps as well as the criterion of $\chi^2/\text{DOF} < 3$ (here the χ^2 is the conventional uncorrelated χ^2, not the correlated χ^2 described in the main text) introduced in previous sections will lead to Figs. 9, 10, and 11. Remarkably, while the outcomes of z shown in Fig. 10 are slightly different from those in Fig. 7, the E_0 and W values presented in Figs. 9 and 11 agree very well with the ones demonstrated in Figs. 6 and 8. In particular, the trend claimed from the analysis associated with the correlated χ^2 regarding the p dependencies of z and W, namely being complementary to each other, is valid as well for the outcomes obtained using the conventional uncorrelated χ^2 (i.e., Figs. 10 and 11). This observation seems to reconfirm the conclusions resulting from investigating some lattice quantum chromodynamics data outlined in Refs. [47,48]. Specifically, using the method of uncorrelated χ^2 to fit correlated data may lead to accurate outcomes for some cases, although the associated χ^2/DOF values cannot truly reflect the quality of the fit.

Interestingly, from the $L = 256$ results shown in Fig. 11, one may conclude that the values of W increase slightly from $p = 0.4$ to $p = 0.6$. This observation would then lead to a (possible) scenario of $p_W = 0.4$. Such a scheme of threshold for W is intriguing since it implies that both p_W and p_z take the same value. Although one cannot definitely rule out the scenario of $p_W = p_z$ (which we call the second scenario), we find it is less favored compared to the one proposed earlier in this study (named the first scenario). This is because the results demonstrated in Fig. 8 (which is obtained by considering the correlation among data), the statistics reached here, and the potential uncertainties due to the errors of $g_c(p)$ indicate that the first scenario seems to be more probable. Nevertheless, it

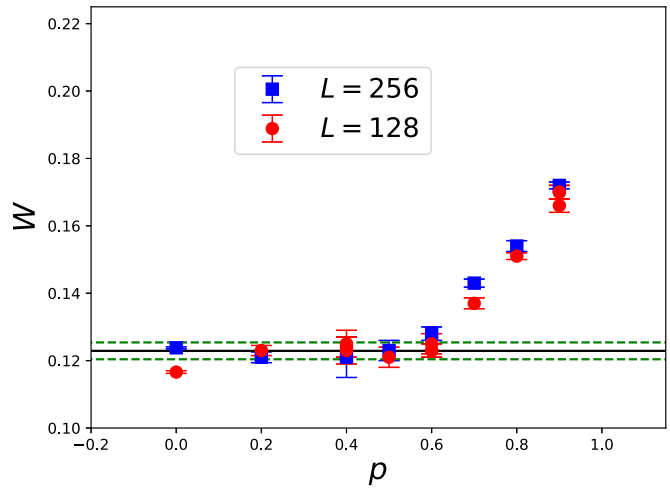

FIG. 11. W as functions of p. The results are obtained from the analysis using the conventional uncorrelated χ^2. The solid squares and solid circles are for $L = 256$ and $L = 128$, respectively. For some values of p, the $L = 128$ results contain those corresponding to g_c, the lower and upper bounds of g_c. The solid and dashed lines in the figure represent the mean and standard deviation for all the values of W such that their corresponding p values satisfy $p < 0.7$ (including both those of $L = 128$ and $L = 256$).

will be extremely interesting to understand the existence of thresholds for z and W, as shown in this investigation, from a theoretical perspective.

To summarize, the outcomes resulting from the investigations carried out here, especially the obtained numerical results of E_0, z, and W, are not only important accomplishments but also can be considered as benchmarks for future related studies.

ACKNOWLEDGMENTS

This study is partially supported by Ministry of Science and Technology of Taiwan.

[1] N. D. Mermin and H. Wagner, Phys. Rev. Lett. **17**, 1133 (1966).
[2] P. C. Hohenberg, Phys. Rev. **158**, 383 (1967).
[3] S. Coleman, Commun. Math. Phys. **31**, 259 (1973).
[4] A. Gelfert and W. Nolting, J. Phys.: Condens. Matter **13**, R505 (2001).
[5] J. Cardy, *Scaling and Renormalization in Statistical Physics* (Cambridge University, Cambridge, England, 1996).
[6] S. Sachdev, *Quantum Phase Transitions*, 2nd ed. (Cambridge University, Cambridge, England, 2011).
[7] S. Chakravarty, B. I. Halperin, and D. R. Nelson, Phys. Rev. B **39**, 2344 (1989).
[8] A. V. Chubukov and S. Sachdev, Phys. Rev. Lett. **71**, 169 (1993).
[9] A. V. Chubukov and S. Sachdev, Phys. Rev. Lett. **71**, 2680(E) (1993).
[10] A. V. Chubukov, S. Sachdev, and J. Ye, Phys. Rev. B **49**, 11919 (1994).
[11] A. W. Sandvik, A. V. Chubukov, and S. Sachdev, Phys. Rev. B **51**, 16483 (1995)
[12] M. Troyer, H. Kontani, and K. Ueda, Phys. Rev. Lett. **76**, 3822 (1996).
[13] M. Troyer, M. Imada, and K. Ueda, J. Phys. Soc. Jpn. **66**, 2957 (1997).
[14] J.-K. Kim and M. Troyer, Phys. Rev. Lett. **80**, 2705 (1998).
[15] Y. J. Kim, R. J. Birgeneau, M. A. Kastner, Y. S. Lee, Y. Endoh, G. Shirane, and K. Yamada, Phys. Rev. B **60**, 3294 (1999).
[16] Y. J. Kim and R. J. Birgeneau, Phys. Rev. B **62**, 6378 (2000).
[17] A. W. Sandvik, V. N. Kotov, and O. P. Sushkov, Phys. Rev. Lett. **106**, 207203 (2011).
[18] A. Sen, H. Suwa, and A. W. Sandvik, Phys. Rev. B **92**, 195145 (2015).
[19] D.-R. Tan and F.-J. Jiang, Phys. Rev. B **98**, 245111 (2018).
[20] F.-J. Jiang, Phys. Rev. B **83**, 024419 (2011).
[21] F.-J. Jiang and U.-J. Wiese, Phys. Rev. B **83**, 155120 (2011).
[22] G. R. Stewart, Rev. Mod. Phys. **56**, 755 (1984).
[23] Z. Zou and P. W. Anderson, Phys. Rev. Lett. **57**, 2073 (1986).
[24] P. Coleman, Heavy fermions: Electrons at the edge of magnetism, in *Handbook of Magnetism and Advanced Magnetic Materials* (Wiley & Sons, Hoboken, NJ, 2007).
[25] V. Gurarie, L. Pollet, N. V. Prokof'ev, B. V. Svistunov, and M. Troyer, Phys. Rev. B **80**, 214519 (2009).
[26] F. Crépin, N. Laflorencie, G. Roux, and P. Simon, Phys. Rev. B **84**, 054517 (2011).
[27] F. Lin, E. S. Sørensen, and D. M. Ceperley, Phys. Rev. B **84**, 094507 (2011).
[28] A. E. Niederle and H. Rieger, New J. Phys. **15**, 075029 (2013).
[29] J.-H. Peng, L.-W. Huang, D.-R. Tan, and F.-J. Jiang, Phys. Rev. B **101**, 174404 (2020).
[30] N. Ma, A. W. Sandvik, and D.-X. Yao, Phys. Rev. B **90**, 104425 (2014).
[31] A. W. Sandvik, Phys. Rev. B **59**, 14157(R) (1999).
[32] A. W. Sandvik, AIP Conf. Proc. **1297**, 135 (2010).
[33] B. Bauer *et al.* (ALPS Collaboration), J. Stat. Mech. (2011) P05001.
[34] http://physics.bu.edu/~sandvik/.
[35] R. Sknepnek, T. Vojta, and M. Vojta, Phys. Rev. Lett. **93**, 097201 (2004).
[36] A. B. Harris, J. Phys. C **7**, 1671 (1974).
[37] J. T. Chayes, L. Chayes, D. S. Fisher, and T. Spencer, Phys. Rev. Lett. **57**, 2999 (1986).
[38] O. Motrunich, S. C. Mau, D. A. Huse, and D. S. Fisher, Phys. Rev. B **61**, 1160 (2000).
[39] A. W. Sandvik, Phys. Rev. Lett. **89**, 177201 (2002).
[40] O. P. Vajk and M. Greven, Phys. Rev. Lett. **89**, 177202 (2002).
[41] R. Yu., T. Roscilde, and S. Haas, Phys. Rev. Lett. **94**, 197204 (2005).
[42] A. W. Sandvik, Phys. Rev. Lett. **96**, 207201 (2006).
[43] T. Vojta, J. Low Temp. Phys. **161**, 299 (2010).
[44] D.-X. Yao, J. Gustafsson, E. W. Carlson, and A. W. Sandvik, Phys. Rev. B **82**, 172409 (2010).
[45] T. Vojta, AIP Conf. Proc. **1550**, 188 (2013).
[46] T. Vojta and J. A. Hoyos, Phys. Rev. Lett. **112**, 075702 (2014).
[47] C. Michael, Phys. Rev. D **49**, 2616 (1994).
[48] C. Michael and A. McKerrell, Phys. Rev. D **51**, 3745 (1995).